Title: Minimal determinants for lifelong antiviral antibody responses from a single exposure to virus-like immunogens at low doses

Authors: Wei-Yun Wholey[1†], Alexander R. Meyer[1†], Sekou-Tidiane Yoda[1], Bryce Chackerian[2], Julie Zikherman[3], Wei Cheng[1,4]*

Affiliations:

[1]*Department of Pharmaceutical Sciences, 428 Church Street, University of Michigan, Ann Arbor, Michigan 48109, USA*

[2]*Department of Molecular Genetics and Microbiology, School of Medicine, University of New Mexico, Albuquerque, New Mexico 87131, USA*

[3]*Division of Rheumatology, Rosalind Russell and Ephraim P. Engleman Rheumatology Research Center, Department of Medicine, University of California, San Francisco, California 94143 USA*

[4]*Department of Biological Chemistry, 1150 W. Medical Center Dr., University of Michigan Medical School, Ann Arbor, Michigan 48109, USA*

*Corresponding author:

Dr Wei Cheng
University of Michigan
428 Church Street
Ann Arbor, MI, 48109-1065
Tel: (734) 763-3709
Fax: (734) 615-6162

email address: chengwe@umich.edu

Keywords: virus-like structure, antibody durability, kinetics, binding, dissociation

†: Both authors contributed equally to this work.

Abstract:

The durability of an antibody (Ab) response is highly important for antiviral vaccines. However, due to the complex compositions of natural virions, the molecular determinants of Ab durability from viral infection or inactivated viral vaccines have been incompletely understood. Here we used a reductionist system of liposome-based virus-like structures to examine the durability of Abs in primary immune responses. This system allowed us to independently vary fundamental viral attributes and to do so without additional adjuvants to model natural viruses. We show that a single injection of antigens (Ags) orderly displayed on a virion-sized liposome is sufficient to induce a long-lived neutralizing Ab (nAb) response. Introduction of internal nucleic acids dramatically modulates the magnitude of long-term Ab responses without alteration of the long-term kinetic trend. These Abs are characterized by exceptionally slow off-rates of ~0.0005 s^{-1}, which emerged as early as day 5 after injection and these off-rates are comparable to that of affinity-matured monoclonal Abs. A single injection of these structures at doses as low as 100 ng led to lifelong nAb production in BALB/c mice. Thus, we have defined the minimal determinants in virus-like immunogens that give rise to potent and long-lasting antiviral Abs from a primary encounter with the host without live infection. This has broad implications for understanding both live viral infection and for optimized vaccine design.

One-sentence summary:

Reconstitution of minimal viral components necessary to trigger durable antiviral IgG

Introduction

The immune system robustly mounts effective Ab responses against a vast range of viral pathogens. This property of the immune response forms the biological basis for many of the vaccines that have been licensed for use in the US. Despite the recent great success of COVID-19 vaccines, there remain challenges that face vaccine development. Among these, a major issue is the durability of protection. At a mechanistic level, conditions that promote the durability of nAb responses are not well understood[1], and the rules that govern the durability of vaccine protection are yet to be defined.[1] Some vaccines, such as those against measles, mumps, and rubella, elicit Abs whose plasma titer half-lives span more than 100 years[2]; in contrast, nAb response wanes quickly even after a second dose of the SARS-CoV-2 mRNA vaccine[3-5], which highlights the importance of booster vaccines for continued protection.

Why do mRNA vaccines require continued boosters to achieve durable protection while certain live attenuated vaccines such as measles and mumps can lead to lifelong protection[2] after only two injections? Currently, we don't have complete answers to this question. However, it has been long recognized that the biophysical form of an Ag is likely to be a critical factor governing Ab durability[6-8]. It has been well documented that multivalent virus-like particles (VLPs) or whole-virus vaccines can induce durable and protective IgG in both preclinical[9] and clinical settings[7]. Prior studies also established that Ag valency has profound impacts on Ab responses compared to monovalent Ags[10-12], including the ability of B cells to differentiate into effector cells[11], clonotype diversity and neutralization breadth[12]. Recently, we have also shown – by contrast to monovalent soluble Ag – that multivalent Ag display on virus-sized liposomes alone, even at a low epitope density, can trigger robust Ag-specific B

cell signaling, survival, and proliferation by evading Lyn-dependent inhibitory pathways for B cell activation[13]. These results indicate that much remains to be learned about mechanisms whereby the biophysical form of an Ag influences the durability of an Ab response.

To understand mechanisms of Ab durability brought by multivalent Ags such as VLPs or whole viruses, one major barrier in our view is the complex ingredients of commonly studied VLPs, as well as the inherent complexity in studies of viral infections, where inflammation[14,15] and cytokine secretion[16] can modulate the immune network to confound Ab responses. Also, for almost all vaccine studies in literature, different adjuvants have been extensively used to induce effective immunity. Under these circumstances, it is difficult to unravel the mechanisms of Ab durability induced by multivalent Ags because the mechanisms of adjuvants have not been completely defined in many cases.

To overcome these limitations, we have developed a reductionist system of synthetic virus-like structures (SVLS) based on liposomes to mimic the complex biophysical features of enveloped viruses[17,18] (also see the companion manuscript). These SVLS are constructed using highly purified biochemical ingredients so that the molecular basis of their immunogenicity is well defined. These SVLS are highly modular in their supramolecular structures so that we can dissect the contributions of critical viral features to the durability of Ab responses by modulating each one independently and collectively. Here, we show that multivalent display of a protein Ag alone on virion-sized liposomes can induce long-lasting production of IgG. Inclusion of internal nucleic acids (iNA) in these structures profoundly modulates the magnitude of IgG in both the immediate and long-term so that a single injection of SVLS at a very low Ag dose can lead to lifelong Ab production in these animals. The Ag-specific IgGs from SVLS immunization are characterized by ultralow off-rates and

offer potent neutralization even when elicited in a T-cell deficient background. These results reveal minimal molecular determinants for a durable Ab response previously observed from live viral infections. The enduring Ab responses as we are about to detail, observed in two entirely different and unrelated protein Ags, indicate that our findings have wide relevance for understanding viruses and developing vaccines.

Results

SVLS induce durable IgG responses

We first conducted a series of immunization studies in both wild-type C57BL/6 (wtB6) and BALB/c mice using the SVLS that we have prepared (the companion manuscript). These SVLS include pRBD and pHEL, the liposomal structures that display the purified receptor binding domain (RBD) of the SARS-CoV-2 S protein or hen egg lysozyme (HEL) without internal nucleic acids (iNA); and pRBD(DNA1) and pHEL(DNA1), which not only display the respective proteins, but also encapsulate DNA1, a 20-mer single-stranded DNA that harbors two unmethylated CpG dinucleotides (Materials and Methods). Throughout, only a single subcutaneous injection was administered at a low submicrogram dose of Ag and the animals were subsequently followed for over one year. Notably, we found that the Ag-specific IgG, in all cases, remains detectable in animal sera over 300 days after the single injection of various SVLS (Fig. 1). As shown in Fig. 1a, the RBD-specific IgG in wtB6 mice elicited by pRBD(DNA1) peaked around 2 months after the exposure and then slowly decayed over time (blue symbols). Without internal DNA1 (triangles), the IgG response was at least 10-fold lower in magnitude, peaked around one month after exposure, and then decayed. However, the level of RBD-specific IgG remained well above the detection limit of the current ELISA, with the lowest concentration of RBD-specific IgG detected as 36±5 ng/ml for sera collected from wtB6 mice on D347 after a single immunization with pRBD3 (upper triangles). The diamonds represent the control sera from wtB6 mice immunized with an irrelevant Ag pHEL(DNA1)1. This control demonstrates that the IgG response is specific towards RBD but not to other components in SVLS such as lipids.

As shown in Fig. 1b, both pRBD (triangles) and pRBD(DNA1) (blue symbols) induced long-lasting IgG whose concentrations in mouse sera increased with time in BALB/c mice, which is in contrast to those in wtB6. The diamonds in Fig. 1b represent the control sera from BALB/c mice immunized with the irrelevant Ag pHEL(DNA1)1, demonstrating the specificity of the IgG responses. With internal DNA1, the concentrations of RBD-specific IgG (blue symbols in Fig. 1b) throughout this period were much higher than those induced by pRBD without iNA (triangles in Fig. 1b), like those in wtB6 and consistent with the notion that innate sensing of Nas controls adaptive immunity[19,20]. As shown in Fig. 1c, sera collected from these immunized animals over this period neutralized more than 95% of pseudovirion infectivity, which included both wtB6 (grey symbols) and BALB/c mice (white symbols), even though the RBD-specific IgG in wtB6 waned over this period of time (Fig. 1a, blue symbols). Control sera from wtB6 immunized with pHEL(DNA1) showed no neutralization of virion infectivity (Fig. 1c, blue diamonds), demonstrating Ag specificity of the neutralizations observed. Continued monitoring of the BALB/c mice immunized with pRBD(DNA1) showed that these nAbs lasted over 600 days (Extended Data Fig. 1a, blue symbols), approaching the life span of these animals recorded in literature[21] and the sera remained highly effective in neutralization of cognate pseudovirions throughout (Extended Data Fig. 1a, white symbols).

Like RBD, qualitatively similar anti-HEL IgG responses were also observed in wtB6 (Fig. 1d) and BALB/c mice (Fig. 1e) upon a single injection of pHEL(DNA1) or pHEL. For all cases in wtB6, the levels of HEL-specific IgG rose initially, which was then followed by slow waning over time. Despite these decays with time, the concentrations of anti-HEL IgG in mouse sera remained well above the limit of detection by the current ELISA. The diamonds in Fig. 1d represent the control sera from wtB6 mice immunized with an irrelevant Ag

pRBD(DNA1)3, demonstrating that the IgG response is specific towards HEL but not to other components in SVLS such as lipids. It is worth noting that the peak concentrations for HEL-specific IgG induced by pHEL(DNA1) (blue symbols in Fig. 1d) were much lower than those for RBD-specific IgG induced by pRBD(DNA1) (blue symbols in Fig. 1a), likely due to the absence of T cell help for HEL in wtB6. As shown in Fig. 1e, both pHEL (triangles) and pHEL(DNA1) (blue symbols) induced long-lasting HEL-specific IgG that increased with time in BALB/c mice, similar to those trends for pRBD and pRBD(DNA1) in BALB/c mice (Fig. 1b) but in contrast to those in wtB6 (Fig. 1d). The diamonds in Fig. 1e represent the control sera from BALB/c mice immunized with the irrelevant Ag pRBD(DNA1)3, demonstrating the specificity of the IgG responses. Also, with internal DNA1, the concentrations of HEL-specific IgG (blue symbols in Fig. 1e) were much higher than those induced by pHEL without iNA (triangles in Fig. 1e), analogous to the situation in Fig. 1b for pRBD(DNA1) in comparison to pRBD in BALB/c mice over the same period of time. Like that of pRBD(DNA1), continued monitoring of the BALB/c mice immunized with pHEL(DNA1) showed that these HEL-specific IgG lasted over 600 days (Extended Data Fig. 1b), suggesting that this lifelong IgG may be a general property that can be achieved for SVLS(DNA1) bearing different foreign Ags. Therefore, a primary Ab response induced by SVLS is long-lasting in both strains of mice. Also, differences in genetic backgrounds contributed substantially to the quantitative evolution of the Ag-specific IgG concentrations with time. The presence of iNA induced a stronger and more durable IgG response compared to SVLS without iNA. Of note, the durable IgG response from pHEL(DNA1) in B6 mice (Fig. 1d blue symbols) suggests that long-lived plasma cells may have been generated in the absence of cognate T cell help[22,23].

Validation of the sensor coating density in BioLayer Interferometry

The rising response of IgG with time in BALB/c mice suggests affinity maturation upon a single injection of a submicrogram dose of Ag in the absence of any other adjuvants. To quantitate the affinity maturation of the IgG responses, we used BioLayer interferometry to directly measure the binding between serum IgG and its target Ag. In our experimental design, a biotinylated Ag was initially loaded onto a streptavidin sensor, and then the sensor was dipped into sera diluted in Buffer 1 (Materials and Methods) to monitor the binding signals in real time. IgG have two Fabs for Ag binding, with bivalent binding of the Ag leading to slower off-rate from the sensor. To assess affinity maturation, it is essential to coat the streptavidin sensor with biotinylated Ag at a low surface density to ensure measurement of monovalent binding and dissociation by IgG. To this end, we first measured binding using a purified commercial monoclonal IgG2a specific for SARS-CoV-2 RBD (BioLegend #944803, mAb1 herein) at three different coating concentrations of biotinylated RBD (Biotin-RBD): 20, 50 and 100 nM. Moreover, the Biotin-RBD was prepared by site-specific biotinylation using the free engineered cysteine near the C-terminus of the RBD (Materials and Methods) to ensure that the epitope on RBD was unmodified. Fig. 2a-b show these binding and dissociation sensorgrams for mAb1. All the dissociation traces in Fig. 2b can be well described by single exponential functions (black lines), which yielded the rate of dissociation for IgG from sensors coated with different concentrations of Biotin-RBD. These observed rate constants from two independent repeats of the same experiments are then plotted in Fig. 2e (black circles) as a function of the concentration of biotin-RBD that was used to coat streptavidin sensors. For these rate constants, a one-way ANOVA test returned a p-value of 0.03428, demonstrating that at the 0.05 level, the population means are significantly different. Specifically, the rate of dissociation from the 100-nM biotin-RBD surface was lower than that of either 20 nM or 50 nM biotin-RBD surface. This result is

consistent with bivalent binding by IgG on streptavidin sensors coated with 100 nM biotin-RBD, but monovalent binding on streptavidin sensors coated with either 20 nM or 50 nM biotin-RBD. To confirm this, we prepared Fab fragments from mAb1 (Materials and Methods) and repeated the binding experiments above at the three different coating concentrations for streptavidin sensors, as shown in Fig. 2c-d. All the dissociation traces in Fig. 2d can be well described by single exponentials (black lines), which yielded the rate of dissociation for Fab fragments from sensors coated with different concentrations of Biotin-RBD. These observed rate constants from two independent repeats of the same experiments are then plotted in Fig. 2e (red circles) as a function of the concentration of biotin-RBD that was used to coat streptavidin sensors. Among these dissociation rate constants for Fab, a one-way ANOVA test returned a p-value of 0.05601, demonstrating that at the 0.05 level, the population means are not significantly different. Specifically, the rate of dissociation from the 100 nM biotin-RBD surface was statistically indistinguishable from that of either the 20 nM or the 50 nM biotin-RBD surface. This result is consistent with monovalent binding by Fab fragments on the streptavidin sensor throughout all three coating conditions. Furthermore, a one-way ANOVA test on the following five sets of rates of dissociation returned a p-value of 0.06043: IgG dissociation from sensors coated with 20 nM biotin-RBD, IgG dissociation from sensors coated with 50 nM biotin-RBD, Fab dissociation from sensors coated with 20 nM biotin-RBD, Fab dissociation from sensors coated with 50 nM biotin-RBD, and Fab dissociation from sensors coated with 100 nM biotin-RBD. This comparison shows that at the 0.05 level, none of these rate constants are significantly different from one another, and thus demonstrates that IgG binds to sensors coated with either 20 or 50 nM biotin-RBD in a monovalent manner. As a consequence, we have chosen 50 nM biotin-RBD or 50 nM biotin-HEL to coat streptavidin sensors for all BioLayer interferometry experiments.

Ag-specific binding kinetics measured using BioLayer interferometry

With the sensor coating density established above, the sera from individual animals at different times post-immunization were then diluted in Buffer 1 and subjected to binding and dissociation measurements with their respective Ags in real time. Representative traces are shown in Fig. 3a and Fig. 3b for sera from a BALB/c mouse immunized with pRBD(DNA1)3 and in Fig. 3c and Fig. 3d for sera from a BALB/c mouse immunized with pHEL(DNA1)1, respectively. The amplitudes from real-time binding and dissociation allowed us to calculate the percentages of Ag-specific IgG that remained bound to Ags at the end of each dissociation period (Extended Data Fig. 2a and 2b), which is a direct indicator of Ab affinity that is largely independent of their input concentrations (Extended Data Fig. 2c). As shown in Fig. 3e, the percentages of Ag-specific IgG that remained bound at the end of dissociation showed a progressive increase until 2 months after the single injection with either pRBD(DNA1) (red symbols) or pHEL(DNA1) (blue symbols), demonstrating affinity maturation. These quantitative trends were in sharp contrast to that for the sera from a B6 $TCR^{-/-}$ mouse that was injected with pHEL(DNA1)1 (green diamonds), which served as a negative control for affinity maturation. Moreover, it is surprising to note that for all cases, regardless of the specific Ags, the off-rates of the Ag-specific IgG induced by either pRBD(DNA1) or pHEL(DNA1) were already at $(5.2\pm0.3)\times10^{-4}$ s^{-1} on Day 5 (D5) (red and blue symbols in Fig. 3f), including the $TCR^{-/-}$ mouse (green diamonds in Fig. 3f). These values of off-rates were comparable to the off-rate of $(3.9\pm0.3)\times10^{-4}$ s^{-1} measured for mAb1, the commercial and affinity-matured mouse monoclonal IgG2a for RBD (Fig. 2e), which is shown as a dashed line in Fig. 3f. This commercial IgG2a can potently block the binding of RBD to human ACE2 at a concentration of 0.05-0.25 μg/mL (BioLegend CAT#944803).

Over the 6-month period after a single injection, the off-rates of the Ag-specific IgG from all these animals underwent little or no changes (Fig. 3f). Thus, the affinity maturation for anti-RBD IgG as indicated in Fig. 3e may be driven primarily by optimization of the Ab on-rate[24,25].

SVLS induce IgG affinity maturation in BALB/c mice

To confirm this, we sought to verify the concentration of Ag-specific IgG in mouse sera (Fig. 1) using an approach that is orthogonal to ELISA. The accurate concentration will then allow us to determine the on-rates without ambiguity. To this end, we first determined the concentration of Ag-specific IgG using a biotinylated Ag pulldown assay with streptavidin-coated magnetic beads (S-beads) followed by quantitative western blotting. These results are shown in Fig. 4a for the capture of RBD-specific IgG on D11 and D123, respectively, from a BALB/c mouse immunized with a single injection of pRBD(DNA1)3 without additional adjuvants. To confirm complete capture of the RBD-specific IgG, we used increasing concentrations of biotin-RBD, as indicated on Lanes 2, 3 and 4 for D11 sera and Lanes 6, 7, and 8 for D123 sera. Comparison with a standard curve (Extended Data Fig. 3) obtained from the same western blots yielded the RBD-specific IgG concentrations for all these samples as shown in the bottom half of Fig. 4a. For D11 sera, Lanes 2, 3 and 4 yielded very similar concentrations, with an average of 0.139±0.007 mg/mL. A one-way ANOVA test among Lanes 2, 3, and 4 returned a p-value of 0.717; therefore, there were no statistically significant differences among these measurements with increasing biotin-RBD, which indicates that we captured nearly all RBD-specific IgG from D11 sera. Also, this concentration was much higher than that measured by ELISA (Fig. 1b), suggesting that the standard curve obtained from affinity-matured mAb1 significantly underestimates the

concentration of anti-RBD IgG on D11. For D123 sera, Lanes 6, 7 and 8 also yielded very similar concentrations, with an average of 0.356±0.007 mg/mL. A one-way ANOVA test among these lanes returned a p-value of 0.96, again demonstrating no statistically significant differences among these measurements with increasing biotin-RBD and indicating that we have captured nearly all RBD-specific IgG from D123 sera. However, a one-way ANOVA test between D11 and D123 measurements returned a p-value of 2.9e-5, indicating that the concentrations of RBD-specific IgG were significantly different in the sera from these two different dates. These concentrations allowed us to measure the on-rates of RBD-specific IgG to RBD using serial dilutions of the respective sera in BioLayer interferometry, as shown in Fig. 4b for the series of binding curves from D11 sera and Fig. 4c for the series of binding curves from D123 sera (note the different scales of the y-axes in Fig. 4b versus 4c). All these binding curves can be well described by exponential functions (solid black lines). We plotted the observed rate constants from these exponential fits as a function of the RBD-specific IgG molar concentration in Fig. 4d, which showed the expected linear dependence for both D11 (grey squares) and D123 sera (cyan circles), with adjusted R-square values of 0.987 for D11 and 0.960 for D123, respectively (straight red lines). The slopes of these lines determined the bi-molecular rate constants for the binding between RBD and RBD-specific IgG, which were $(4.2\pm0.2)\times10^{4}$ $M^{-1}s^{-1}$ on D11 and $(1.2\pm0.1)\times10^{5}$ $M^{-1}s^{-1}$ on D123. Therefore, the binding rate constants increased almost 3-fold over the period from D11 to D123, demonstrating affinity maturation.

Discussion

(1) The minimal molecular determinants for a durable Ab response

Acute live viral infection in mice can lead to long-lasting antiviral serum Abs in both B6 and BALB/c mice[26]. At present, the mechanistic linkage between immediate and long-term Ab production upon viral infection or vaccination has not been fully established[27,28]. This is due in part to the inherent complexity of studies of viral infections, as well as the empirical use of adjuvants or the complex ingredients of commonly studied VLPs. In many cases, a single injection of an immunogen in the absence of adjuvants is expected to produce a short-term Ab response only. In light of this background, it is notable that the IgG responses to a single injection of SVLS at a very low Ag dose were long-lived, regardless of the displayed protein Ag or the mouse genetic background (Fig. 1). Immunization with SVLS not only initiated rapid IgG responses, but also promoted the long-term production of IgG. In BALB/c mice, a single immunization with SVLS leads to lifelong secretion of IgG (Extended Data Fig. 1), regardless of the specific protein Ag. These results indicate that ED above a threshold on a virus-sized structure, in the absence of any other adjuvants or TLR activation, can deliver long-term survival signals for Ag-specific plasma cells, true for both B6 and BALB/c mice. The presence of iNA can profoundly modulate the magnitude of the IgG response in both the short and long-term. These data thus established the minimal determinants in virus particles that give rise to long-lasting antiviral Ab responses from a primary encounter with the host. Overall, these results are consistent with the models in literature that Ag valency together with antigenic threshold may determine the durability of a protective Ab response[7].

However, the differences in the long-term trends of IgG in response to the same immunogens at the same Ag dose between mouse strains are also intriguing. Within the same strain, regardless of the specific Ags or the inclusion of iNA, the evolution of IgG with time followed the same up or down trends (Fig. 1). Therefore, the differences in long-term Ab responses appear to be more related to strain differences instead of the specific Ags or TLR

signaling. Along this line of strain differences, we noted that BALB/c mice mounted much stronger IgG1 than wtB6 on D11 for both pRBD and pHEL (the companion manuscript, Fig. 6), even though the levels of Ag-specific IgG were overall comparable on D5 between the two strains of mice (the companion manuscript, Fig. 2j). These results suggest that early on in an Ab response to virus-like immunogens (between D5 and D11), BALB/c mice amplify the activation signals conveyed by epitope density more than wtB6. Whether this difference observed on D11 may lead to differences in IgG long-term trends between the two strains remains to be studied. Moreover, what causes these differences between wtB6 and BALB/c towards the same SVLS? Among several possibilities, whether these differences are imparted from the original Ag exposure[7] (differences in B cell precursor frequency for example) or due to differences that occur at a later stage after the initial B cell activation and MHC class II Ag presentation[29] remain to be tested. Table S1 summarizes the initiation and durability of IgG responses from current studies together with their implications for the understanding of viral Ab response in mice.

(2) Virus-like immunogens elicit T-independent IgG with exceptional off-rate.

Another surprising result from the current study is that these rapidly produced Ag-specific IgG elicited by SVLS exhibit very slow off-rates that are less than 0.001 s^{-1}, which are comparable to that of a commercial affinity-matured mAb (Fig. 3f). These IgGs emerged as early as Day 5 post Ag exposure, regardless of the specific protein Ag or the mice strains and even in the absence of functional T cells (Fig. 3f). The IgG from both B6 and BALB/c mice can potently neutralize cognate pseudovirions (Fig. 1c). These data are consistent with previous studies of live infection by vesicular stomatitis virus (VSV) and influenza virus in murine models. It has been found that VSV-specific IgG in germline configuration is already

highly protective against VSV infection[30], which does not require somatic hypermutation or affinity maturation[30]. Similar results also occur in murine models of influenza virus infection[31]. The current study offers a mechanistic explanation for these live infection data: (1) live infection produces virions; (2) the consensus features of virion structures, i.e., epitope density (ED) and iNA in the context of a virion-sized structure, can robustly activate naïve Ag-specific B cells to initiate class-switch recombination and secrete IgG that is independent of viral replication or any other adjuvants; and (3) the IgG has an intrinsically slow off-rate that can offer effective neutralization of cognate virions. The slow IgG off-rates that we observed even for a nonviral protein, HEL (Fig. 3f) suggests that this may be a general phenomenon in mice upon induction by a virus-like immunogens.

An optimal, highly potent IgG should have both a fast on-rate and a very slow off-rate so that it can bind its target with high affinity. Despite a very slow off-rate, this early version of RBD-specific IgG is not optimal because of a slow on-rate. As shown in Fig. 4d, the RBD-specific IgG on D11 post injection has an on-rate of $(4.2\pm0.2)\times10^4$ $M^{-1}s^{-1}$, which is more than tenfold slower than the on-rate of the commercial RBD-specific mAb1 that we have measured, $(6.1\pm0.3)\times10^5$ $M^{-1}s^{-1}$ (data not shown). However, we hypothesize that this immediate IgG response is at evolutionary advantage to the host because defects in IgG on-rate can be potentially compensated for by a high concentration of the IgG rapidly secreted in the context of an extra-follicular response to acute viral infection, which is triggered by the combined signals from ED and iNA presented by intact virion structures. This suggests that upon germinal center formation in a suitable host, the major improvements conferred by affinity maturation to these IgGs are likely in the on-rates of Ag binding. In fact, this is the case in our data (Fig. 4d): over a period of 2 months, the on-rate of the RBD-specific IgG increased by roughly 3-fold from the single injection. Also, in murine models of live

infection by VSV, it was discovered that the efficiency of virion neutralization is highly correlated with the on-rates of viral-specific IgGs identified throughout the live viral infection[25,32], suggesting that this optimization of IgG on-rate is indeed the case for live viral infections. In a separate study, enhancement of IgG on-rate during affinity maturation was also observed for human nAbs induced upon infection by the respiratory syncytial virus[24]. Therefore, in both mice and humans, live infections of two different viruses optimized the on-rate of IgG, suggesting that the germline progenitor of this IgG has excellent off-rates to provide effective protection. Taken together, this is a highly effective strategy for antiviral defense. The speed and magnitude of this IgG response are largely independent of T cells, affording the host with a mechanism for a fast and strong nAb response that would be critical during the early onset[33] of an antiviral defense. It's important to note that, in addition to binding rates, an IgG's potency for neutralizing viral infectivity is also influenced by the virus' ED. Specifically, the ED of the virus can impact the stability and effectiveness of bivalent binding by the IgG, which is more effective than monovalent binding[34,35].

(3) SVLS as new platform for dissection of antiviral response and potential vaccines.

In comparison to the complex bacteriophage VLPs that have been used in studies of Ab responses to virus-like immunogens, SVLS use the minimal essential viral components to model these Ags, yet the potency of the IgG response triggered by these SVLS can be compared to that of well-established bacteriophage VLPs (see the companion manuscript), suggesting that this platform has captured the key features of VLPs which trigger an Ab response. This platform is highly modular and can be readily adapted to different proteins. We have tested RBD and HEL as shown in the current study and a self-Ag peptide previously[36]. Therefore, this platform has the potential for use in other viral protein systems

for understanding Ab responses without an active infection, as well as potential applications in vaccines. The modular nature of the SVLS structure is particularly desirable for dissecting the roles of individual components in Ab responses towards complex immunogens such as virions. The completely synthetic nature of these SVLS could also be useful for vaccine design and formulation from several different perspectives. First, the ability to use iNA for intrinsic TLR activation can dramatically enhance B cell activation, which may be strongly desired for activating those very rare Ag-specific B cells. In this regard, SVLS may be at an advantage compared to lumazine synthase[37], ferritin nanoparticles[38] or computationally designed self-assembling protein nanomaterials[39]. Second, SVLS use a stable formulation[17,18] to preserve the integrity of virus-like structures for presentation of protein Ags in their native conformations without any associated viral infectivity, which may be at an advantage compared to inactivated viruses, where formaldehyde and/or detergent treatment can alter conformations of protein Ags or even destroy the structures of viruses that are critical for B cell activation[7]. Third, the regulatory requirements for purified synthetic agents could be less complex compared to products directly derived from cell culture[40], and last, the use of nucleic acids with native phosphodiester backbones in SVLS without the need for nuclease-resistant phosphorothioate could substantially reduce the cost of vaccine manufacture.

MATERIALS AND METHODS

Synthesis of SVLS

All SVLS used throughout this study were prepared following protocols we published previously[17,18,36]. These SVLS were constructed using nonimmunogenic lipids, with phosphatidylcholine and cholesterol comprising ≥ 99% of all lipids. These structures display protein antigens (Ags) of choice in a specific orientation on their surfaces with a regulated ED that quantitatively mimics the surface of naturally occurring viruses[34,41]. The HEL recombinant protein used in this study contains two site-directed mutations at R73E and D101R and was overexpressed in *E. coli* and purified to >95% purity following our established protocols[17]. The SARS-CoV-2 RBD recombinant protein used in this study was overexpressed using 293F cells and purified to >95% purity following our established protocols[18]. DNA1 was custom synthesized by IDT. The sequence of DNA1 is as follows, 5'-TCCATGA<u>CG</u>TTCCTGA<u>CG</u>TT-3'. Epitope density (ED) was quantified using methods that we established previously [17,18,36,42] that were also validated by single-molecule fluorescence techniques that were developed and established in house[43,44]. For SVLS with iNA, the average number of iNA molecules per SVLS was also quantified using methods that we established previously[17,18].

Mice immunizations

All animal procedures were approved by the University of Michigan Animal Care and Use Committee. Female C57BL/6 or BALBc/J mice (8 weeks, Jackson Laboratory) were used for immunizations. Prior to inoculation, all injection samples were filtered through a 0.45 µm

pore size membrane to eliminate potential microbial contamination. 100 µL samples at a dose between 0.1 and 0.48 µg of respective protein Ags were injected into each mouse subcutaneously, 50 µL in each flank. Throughout the entire study, no adjuvants other than the SVLS were administered unless otherwise noted and only a single injection was administered throughout. Mouse blood was collected submentally using Microvette serum collection tubes (Sarstedt) three days before the first injection, and 5 days thereafter following specified blood collection schedules. The sera were harvested by centrifugation at 10,000 g for 5 minutes, aliquoted and immediately frozen and stored at -80°C.

Enzyme-Linked Immunosorbent Assay (ELISA)

Blood serum was tested by ELISA in order to quantitate Ag-specific IgG responses to various immunizations. 96-well plates (Nunc MaxiSorp, Invitrogen) were coated overnight at 4°C with either 200 ng of sHEL or 320 ng of sRBD per well in PBS. After blocking with 1% Bovine Serum Albumin (BSA, Fisher) in PBS, mouse sera of specified dilution factors were added to each well for incubation at 22°C for 2 hours. After three washes using PBS with 0.05% Tween 20, secondary goat anti-mouse IgG Fc-HRP antibody (# 1033-05, SouthernBiotech) was added in blocking buffer at 1:6000 dilution and incubated for 1 hour at 22°C. Following three washes, 100 µL of substrate 3,3',5,5'-Tetramethylbenzidine (Thermo Scientific) was added to each well and incubated in the dark for 10 minutes. The reaction was stopped by addition of 100 µL 2M sulfuric acid in each well. The optical density of each well at 450 nm was measured using a microplate reader (Bio-Tek Synergy HT). All the OD values reported were background subtracted by comparison between two wells that were coated with soluble protein and PBS, respectively. To estimate Ag-specific IgG concentrations in mouse sera based on ELISA standard curves, all sera samples were properly

diluted to reach final OD values between 0.2 and 0.5 before interpolation. The Extended Data Fig. 2 in the companion manuscript shows a representative set of standard curves. Specifically, we used mAb1, the commercial RBD-specific monoclonal mouse IgG2a (BioLegend CAT#944803) as the known reference to construct standard curves for detection of RBD-specific IgG and IgG2a. We used mAb2, the HEL-specific monoclonal mouse IgG1 (clone HyHEL10, a special gift from Prof. Irina Grigorova) as the known reference to construct standard curves for detection of HEL-specific IgG and IgG1.

Preparation of HIV-1 virions pseudotyped with SARS-CoV-2 envelope

The HIV-1 pseudotyped with SARS-CoV-2 envelope was prepared following published protocols [45] but with modifications. Briefly, HEK 293T/17 cells (ATCC, Manassas, VA) were cultured at 37°C with 5% CO_2 in DMEM supplemented with 10% FBS (HyClone Laboratories, Logan, UT). 10^6 293T cells in a 2-mL culture volume were seeded overnight in a 35-mm dish before transfection using the TransIT LT-1 transfection reagent (Mirus Bio, Madison, WI). For each dish, 2 μg of the provirus-containing plasmid pNL4-3 luc R^-E^- [46] (ARP-3418, NIH AIDS Research and Reference Reagent Program) was used to make the transfection reagent mixture, together with 1 μg of envelope expression plasmid pcDNA3.1 SARS-CoV-2 S D614G [45]. The plasmid pcDNA3.1 SARS-CoV-2 S D614G was a gift from Jeremy Luban (Addgene plasmid # 158075; http://n2t.net/addgene:158075; RRID:Addgene_158075). The RBD amino acid sequence 328-537 encoded in this plasmid is identical to the sequence of RBD that we studied here. The transfection reagent mixture was incubated at room temperature for 15 min before drop wise addition to the culture medium, as we did previously [47]. At 6 hours post transfection, the culture medium together with the transfection reagents was replaced with fresh complete medium and the incubation was

continued at 37°C with 5% CO_2. At 48 hours post transfection, the entire culture medium containing single-cycle HIV-1 viruses was collected and filtered through a 0.45-μm syringe filter (Millex-HV PVDF, Millipore). The filtrate was then aliquoted on ice, flash-frozen in liquid nitrogen and stored in a -80°C freezer. The concentration of virion particles was quantitated using a HIV-1 p24 ELISA kit (CAT#XB-1000, XpressBio) as we described previously [47].

Virion neutralization assay

The virion neutralization assay follows the protocols we established previously but with important modifications [47]. HIV-1 virions pseudotyped with SARS-CoV-2 envelope containing 9 ng of HIV-1 p24 were incubated with various mouse sera at 37°C for one hour, and then diluted with complete medium by 8-fold in volume for the sera to initiate infection of Huh-7.5 cells at 37°C for 2 hours. At the end of 2 hours, fresh medium was added to each well in a 24-well plate and the incubation was continued at 37°C with 5% CO_2. Luciferase activity was measured 48 hours after infection. Briefly, the culture medium was removed and replaced with 100 μL of complete medium. 100 μL of Bright-Glo™ reagent (CAT#E2610, Promega) that was just warmed to room temperature was then added to each well. The cells were incubated for three minutes at room temperature to allow cell lysis. After three minutes, 100 μL of lysate from each well was transferred to a single well in a 96-well black microtiter plate (Costar). Luminescence was measured using a Synergy™ HT multi-mode plate reader (BioTek Instruments Inc., Vermont) and background luminescence was subtracted using Huh-7.5 cells without virus infection. For comparison among different time points post immunization, the luminescence readings for cells incubated with sera from each group of mice before injections was set as 100%. The luminescence readings from other time points

for the same group were all normalized based on this and plotted as a percentage of remaining infectivity.

BioLayer interferometry measurements

Affinity maturation of Ag-specific antibodies in animal sera together with binding and dissociation rate constants were measured using BioLayer interferometry. Briefly, the streptavidin sensor (Sartorius Corp) was coated with 50 nM Biotin-RBD or Biotin-HEL in 1×PBS for 30 min at 20°C, which was followed by washing in PBS for 10 min. For this application, both RBD and HEL were site-specifically biotinylated in house using EZ-link maleimide-PEG2-biotin (ThermoFisher, CAT#A39261) so that the binding epitopes on these proteins were not modified. After sensor loading, they were dipped into antibodies or sera of varied dilutions in Buffer 1 to measure the binding in real time using an OctetRed BioLayer Interferometer equipped with 8 sensor positions that were read simultaneously. The measurement for binding was continued for the indicated time, which was followed by dipping the sensors into Buffer 1 for the indicated time to monitor the dissociation in real time. Throughout, the measurements were done at 20°C. A PBS coated sensor control was included and subtracted from all the kinetic data before quantitative analysis. Buffer 1 was 1×PBS with 0.05% Tween 20 and 0.1% BSA. The percentage of IgG remaining bound, p, was determined by using the amplitude information from both binding and dissociation curves, specifically as follows: $p=(A1+A2)/A1*100\%$, in which A1, a positive number, is the final amplitude at the end of binding measurement, and A2, a negative number as the result of dissociation, is the final amplitude at the end of dissociation measurement, as illustrated in Extended Data Fig. 2a and 2b. In the current study, most binding and dissociation events were measured continuously in real time for 50 min each. For experiments shown in Fig. 4,

the binding and dissociation were monitored continuously for 4000 s for better definition of the rate constants. The control Fab was prepared from the IgG form of the antibody (mAb1) using a Pierce™ Fab Micro preparation kit (ThermoFisher Scientific, CAT#44685) following manufacturer instructions.

Measurement of Ag-specific IgG concentration in animal sera using magnetic beads

We measured the concentration of Ag-specific IgG in the sera of immunized animals using streptavidin-coated magnetic beads. Specifically, high capacity Magne streptavidin beads (Promega CAT#V7820) were first exchanged into PBS buffer, and then mixed with biotinylated RBD or HEL for binding at 20°C for 1 hr with constant mixing on a lab vortexer. After this, the beads were washed 3 times using Buffer 1 and then mixed with sera also diluted in Buffer 1. The binding was continued at 20°C for 2 hrs with constant mixing. Finally, the supernatant was removed, and the bound IgG was resuspended in nonreducing Laemmli sample buffer at 95°C for 10 min. The amount of Ag-specific IgG was then quantitated by running a western blot using mouse IgG (BioLegend CAT#944803) of known mass as a standard. The secondary antibody used was goat anti-mouse IgG (Fc specific) conjugated with alkaline phosphatase from Sigma (CAT#A1418) and used at 1:3000 dilution.

Statistical analysis

Statistical analysis was carried out using the Statistics toolbox in MATLAB (Mathworks, MA). A comparison of two independent variables was carried out using a two-sample T-test. Data sets with more than two independent variables were analyzed using a one-way analysis of variance as indicated. P-values less than 0.05 were considered statistically significant.

Throughout, all errors in the main text were reported as standard errors unless otherwise noted; all data points in figures were reported as mean ± standard error unless otherwise noted.

References

1 Palin, A. C. *et al.* The persistence of memory: defining, engineering, and measuring vaccine durability. *Nat Immunol* **23**, 1665-1668 (2022). https://doi.org:10.1038/s41590-022-01359-z

2 Amanna, I. J., Carlson, N. E. & Slifka, M. K. Duration of humoral immunity to common viral and vaccine antigens. *N Engl J Med* **357**, 1903-1915 (2007). https://doi.org:10.1056/NEJMoa066092

3 Korosec, C. S. *et al.* Long-term durability of immune responses to the BNT162b2 and mRNA-1273 vaccines based on dosage, age and sex. *Sci Rep* **12**, 21232 (2022). https://doi.org:10.1038/s41598-022-25134-0

4 Gupta, S. L. *et al.* Loss of Pfizer (BNT162b2) Vaccine-Induced Antibody Responses against the SARS-CoV-2 Omicron Variant in Adolescents and Adults. *J Virol* **96**, e0058222 (2022). https://doi.org:10.1128/jvi.00582-22

5 Anderson, M. *et al.* Longitudinal Severe Acute Respiratory Syndrome Coronavirus 2 Vaccine Antibody Responses and Identification of Vaccine Breakthrough Infections Among Healthcare Workers Using Nucleocapsid Immunoglobulin G. *J Infect Dis* **226**, 1934-1942 (2022). https://doi.org:10.1093/infdis/jiac420

6 Slifka, M. K. & Ahmed, R. Long-term humoral immunity against viruses: revisiting the issue of plasma cell longevity. *Trends Microbiol* **4**, 394-400 (1996). https://doi.org:10.1016/0966-842X(96)10059-7

7 Slifka, M. K. & Amanna, I. J. Role of Multivalency and Antigenic Threshold in Generating Protective Antibody Responses. *Front Immunol* **10**, 956 (2019). https://doi.org:10.3389/fimmu.2019.00956

8 Bhattacharya, D. Instructing durable humoral immunity for COVID-19 and other vaccinable diseases. *Immunity* **55**, 945-964 (2022). https://doi.org:10.1016/j.immuni.2022.05.004

9 Chackerian, B., Lowy, D. R. & Schiller, J. T. Conjugation of a self-antigen to papillomavirus-like particles allows for efficient induction of protective autoantibodies. *J Clin Invest* **108**, 415-423 (2001). https://doi.org:10.1172/JCI11849

10 Dintzis, H. M., Dintzis, R. Z. & Vogelstein, B. Molecular determinants of immunogenicity: the immunon model of immune response. *Proc Natl Acad Sci U S A* **73**, 3671-3675 (1976).

11 Kato, Y. *et al.* Multifaceted Effects of Antigen Valency on B Cell Response Composition and Differentiation In Vivo. *Immunity* (2020). https://doi.org:10.1016/j.immuni.2020.08.001

12 Ols, S. *et al.* Multivalent antigen display on nanoparticle immunogens increases B cell clonotype diversity and neutralization breadth to pneumoviruses. *Immunity* **56**, 2425-2441 e2414 (2023). https://doi.org:10.1016/j.immuni.2023.08.011

13 Brooks, J. F. *et al.* Molecular basis for potent B cell responses to antigen displayed on particles of viral size,DOI 10.1038/s41590-023-01597-9. *Nat Immunol* (2023). https://doi.org:10.1038/s41590-023-01597-9

14 Sefik, E. *et al.* Inflammasome activation in infected macrophages drives COVID-19 pathology. *Nature* **606**, 585-593 (2022). https://doi.org:10.1038/s41586-022-04802-1

15 Merad, M., Blish, C. A., Sallusto, F. & Iwasaki, A. The immunology and immunopathology of COVID-19. *Science* **375**, 1122-1127 (2022). https://doi.org:10.1126/science.abm8108

16 Zhang, Q., Bastard, P., Effort, C. H. G., Cobat, A. & Casanova, J. L. Human genetic and immunological determinants of critical COVID-19 pneumonia. *Nature* **603**, 587-598 (2022). https://doi.org:10.1038/s41586-022-04447-0

17 Wholey, W. Y. *et al.* Synthetic Liposomal Mimics of Biological Viruses for the Study of Immune Responses to Infection and Vaccination. *Bioconjug Chem* **31**, 685-697 (2020). https://doi.org:10.1021/acs.bioconjchem.9b00825

18 Wholey, W. Y., Yoda, S. T. & Cheng, W. Site-Specific and Stable Conjugation of the SARS-CoV-2 Receptor-Binding Domain to Liposomes in the Absence of Any Other Adjuvants Elicits

Potent Neutralizing Antibodies in BALB/c Mice. *Bioconjug Chem* **32**, 2497-2506 (2021). https://doi.org:10.1021/acs.bioconjchem.1c00463
19 Iwasaki, A. & Medzhitov, R. Regulation of adaptive immunity by the innate immune system. *Science* **327**, 291-295 (2010). https://doi.org:10.1126/science.1183021
20 Iwasaki, A. & Medzhitov, R. Control of adaptive immunity by the innate immune system. *Nat Immunol* **16**, 343-353 (2015). https://doi.org:10.1038/ni.3123
21 Goodrick, C. L. Life-span and the inheritance of longevity of inbred mice. *J Gerontol* **30**, 257-263 (1975). https://doi.org:10.1093/geronj/30.3.257
22 Bortnick, A. *et al.* Long-lived bone marrow plasma cells are induced early in response to T cell-independent or T cell-dependent antigens. *J Immunol* **188**, 5389-5396 (2012). https://doi.org:10.4049/jimmunol.1102808
23 Taillardet, M. *et al.* The thymus-independent immunity conferred by a pneumococcal polysaccharide is mediated by long-lived plasma cells. *Blood* **114**, 4432-4440 (2009). https://doi.org:10.1182/blood-2009-01-200014
24 Bates, J. T. *et al.* Reversion of somatic mutations of the respiratory syncytial virus-specific human monoclonal antibody Fab19 reveal a direct relationship between association rate and neutralizing potency. *J Immunol* **190**, 3732-3739 (2013). https://doi.org:10.4049/jimmunol.1202964
25 Foote, J. & Eisen, H. N. Kinetic and affinity limits on antibodies produced during immune responses. *Proc Natl Acad Sci U S A* **92**, 1254-1256 (1995). https://doi.org:10.1073/pnas.92.5.1254
26 Slifka, M. K., Matloubian, M. & Ahmed, R. Bone marrow is a major site of long-term antibody production after acute viral infection. *J Virol* **69**, 1895-1902 (1995). https://doi.org:10.1128/JVI.69.3.1895-1902.1995
27 Lam, J. H. & Baumgarth, N. The Multifaceted B Cell Response to Influenza Virus. *J Immunol* **202**, 351-359 (2019). https://doi.org:10.4049/jimmunol.1801208
28 Robinson, M. J. *et al.* Intrinsically determined turnover underlies broad heterogeneity in plasma-cell lifespan. *Immunity* **56**, 1596-1612 e1594 (2023). https://doi.org:10.1016/j.immuni.2023.04.015
29 Pishesha, N., Harmand, T. J. & Ploegh, H. L. A guide to antigen processing and presentation. *Nat Rev Immunol* **22**, 751-764 (2022). https://doi.org:10.1038/s41577-022-00707-2
30 Kalinke, U. *et al.* The role of somatic mutation in the generation of the protective humoral immune response against vesicular stomatitis virus. *Immunity* **5**, 639-652 (1996). https://doi.org:10.1016/s1074-7613(00)80277-0
31 Lam, J. H., Smith, F. L. & Baumgarth, N. B Cell Activation and Response Regulation During Viral Infections. *Viral Immunol* **33**, 294-306 (2020). https://doi.org:10.1089/vim.2019.0207
32 Roost, H. P. *et al.* Early high-affinity neutralizing anti-viral IgG responses without further overall improvements of affinity. *Proc Natl Acad Sci U S A* **92**, 1257-1261 (1995). https://doi.org:10.1073/pnas.92.5.1257
33 Lam, J. H. & Baumgarth, N. Toll-like receptor mediated inflammation directs B cells towards protective antiviral extrafollicular responses. *Nat Commun* **14**, 3979 (2023). https://doi.org:10.1038/s41467-023-39734-5
34 Klein, J. S. & Bjorkman, P. J. Few and far between: how HIV may be evading antibody avidity. *PLoS Pathog* **6**, e1000908 (2010). https://doi.org:10.1371/journal.ppat.1000908
35 Galimidi, R. P. *et al.* Intra-spike crosslinking overcomes antibody evasion by HIV-1. *Cell* **160**, 433-446 (2015). https://doi.org:10.1016/j.cell.2015.01.016
36 Chen, Z. *et al.* Self-Antigens Displayed on Liposomal Nanoparticles above a Threshold of Epitope Density Elicit Class-Switched Autoreactive Antibodies Independent of T Cell Help. *J Immunol* **204**, 335-347 (2020). https://doi.org:10.4049/jimmunol.1801677
37 Zhang, X., Meining, W., Fischer, M., Bacher, A. & Ladenstein, R. X-ray structure analysis and crystallographic refinement of lumazine synthase from the hyperthermophile Aquifex

aeolicus at 1.6 A resolution: determinants of thermostability revealed from structural comparisons. *J Mol Biol* **306**, 1099-1114 (2001). https://doi.org:10.1006/jmbi.2000.4435

38 Yamashita, I., Iwahori, K. & Kumagai, S. Ferritin in the field of nanodevices. *Biochim Biophys Acta* **1800**, 846-857 (2010). https://doi.org:10.1016/j.bbagen.2010.03.005

39 King, N. P. *et al.* Computational design of self-assembling protein nanomaterials with atomic level accuracy. *Science* **336**, 1171-1174 (2012). https://doi.org:10.1126/science.1219364

40 Bridges, C. B. *et al.* Prevention and control of influenza. Recommendations of the Advisory Committee on Immunization Practices (ACIP). *MMWR Recomm Rep* **52**, 1-34; quiz CE31-34 (2003).

41 Cheng, W. The Density Code for the Development of a Vaccine? *J Pharm Sci* **105**, 3223-3232 (2016). https://doi.org:10.1016/j.xphs.2016.07.020

42 Chen, Z., Moon, J. J. & Cheng, W. Quantitation and Stability of Protein Conjugation on Liposomes for Controlled Density of Surface Epitopes. *Bioconjug Chem* **29**, 1251-1260 (2018). https://doi.org:10.1021/acs.bioconjchem.8b00033

43 Pang, Y., Song, H., Kim, J. H., Hou, X. & Cheng, W. Optical trapping of individual human immunodeficiency viruses in culture fluid reveals heterogeneity with single-molecule resolution. *Nat Nanotechnol* **9**, 624-630 (2014). https://doi.org:nnano.2014.140 [pii]

10.1038/nnano.2014.140

44 DeSantis, M. C., Kim, J. H., Song, H., Klasse, P. J. & Cheng, W. Quantitative Correlation between Infectivity and Gp120 Density on HIV-1 Virions Revealed by Optical Trapping Virometry. *J Biol Chem* **291**, 13088-13097 (2016). https://doi.org:10.1074/jbc.M116.729210

45 Yurkovetskiy, L. *et al.* Structural and Functional Analysis of the D614G SARS-CoV-2 Spike Protein Variant. *Cell* **183**, 739-751 e738 (2020). https://doi.org:10.1016/j.cell.2020.09.032

46 Connor, R. I., Chen, B. K., Choe, S. & Landau, N. R. Vpr is required for efficient replication of human immunodeficiency virus type-1 in mononuclear phagocytes. *Virology* **206**, 935-944 (1995). https://doi.org:10.1006/viro.1995.1016

47 Kim, J. H., Song, H., Austin, J. L. & Cheng, W. Optimized Infectivity of the Cell-Free Single-Cycle Human Immunodeficiency Viruses Type 1 (HIV-1) and Its Restriction by Host Cells. *PLoS One* **8**, e67170 (2013). https://doi.org:10.1371/journal.pone.0067170

48 Hangartner, L., Zinkernagel, R. M. & Hengartner, H. Antiviral antibody responses: the two extremes of a wide spectrum. *Nat Rev Immunol* **6**, 231-243 (2006). https://doi.org:10.1038/nri1783

49 Szomolanyi-Tsuda, E. & Welsh, R. M. T-cell-independent antiviral antibody responses. *Curr Opin Immunol* **10**, 431-435 (1998). https://doi.org:10.1016/s0952-7915(98)80117-9

50 Lee, B. O. *et al.* CD4 T cell-independent antibody response promotes resolution of primary influenza infection and helps to prevent reinfection. *J Immunol* **175**, 5827-5838 (2005).

51 Juleff, N. *et al.* Foot-and-mouth disease virus can induce a specific and rapid CD4+ T-cell-independent neutralizing and isotype class-switched antibody response in naive cattle. *J Virol* **83**, 3626-3636 (2009). https://doi.org:10.1128/JVI.02613-08

52 Wang, L. C. *et al.* CD4 T-cell-independent antibody response reduces enterovirus 71 lethality in mice by decreasing tissue viral loads. *Clin Dev Immunol* **2012**, 580696 (2012). https://doi.org:10.1155/2012/580696

Acknowledgements:

We thank Prof. Irina Grigorova for critical reading of the work during the early development of the manuscript. We thank Prof. Marilia Cascalho for very helpful discussion regarding the data and this work. We thank Dr. Charlie Rice at Rockefeller University for the kind gift of Huh-7.5 cells. The following reagent was obtained through the AIDS Research and Reference Reagent Program, Division of AIDS, National Institute of Allergy and Infectious Diseases (NIAID), National Institutes of Health (NIH): pNL4-3.Luc.R-E- from Dr. Nathaniel Landau. The plasmid pcDNA3.1 SARS-CoV-2 S D614G was a gift from Dr. Jeremy Luban through Addgene.

Funding:

NIH/NIAID grant 1R01AI155653-01A1 (WC, JZ), NIH/NIGMS T32 GM145304 Cellular Biotechnology Training Program (ARM).

Author contributions:

Conceptualization: WC
Methodology: WW, ARM, SY, WC
Investigation: WW, ARM, SY, WC
Visualization: WW, ARM, WC
Funding acquisition: WC, JZ
Project administration: WC
Supervision: WC
Writing: WW, ARM, BC, JZ, WC

Competing interests

W. Cheng has a patent pending on SVLS. B. Chackerian has equity in Flagship Laboratories 72. J. Zikherman is on the scientific advisory board for Walking Fish Therapeutics. No other disclosures were reported.

Data and materials availability:

All data are available in the main text or the supplementary materials.

Additional Materials

Extended Data Figs. 1 to 3

Figures

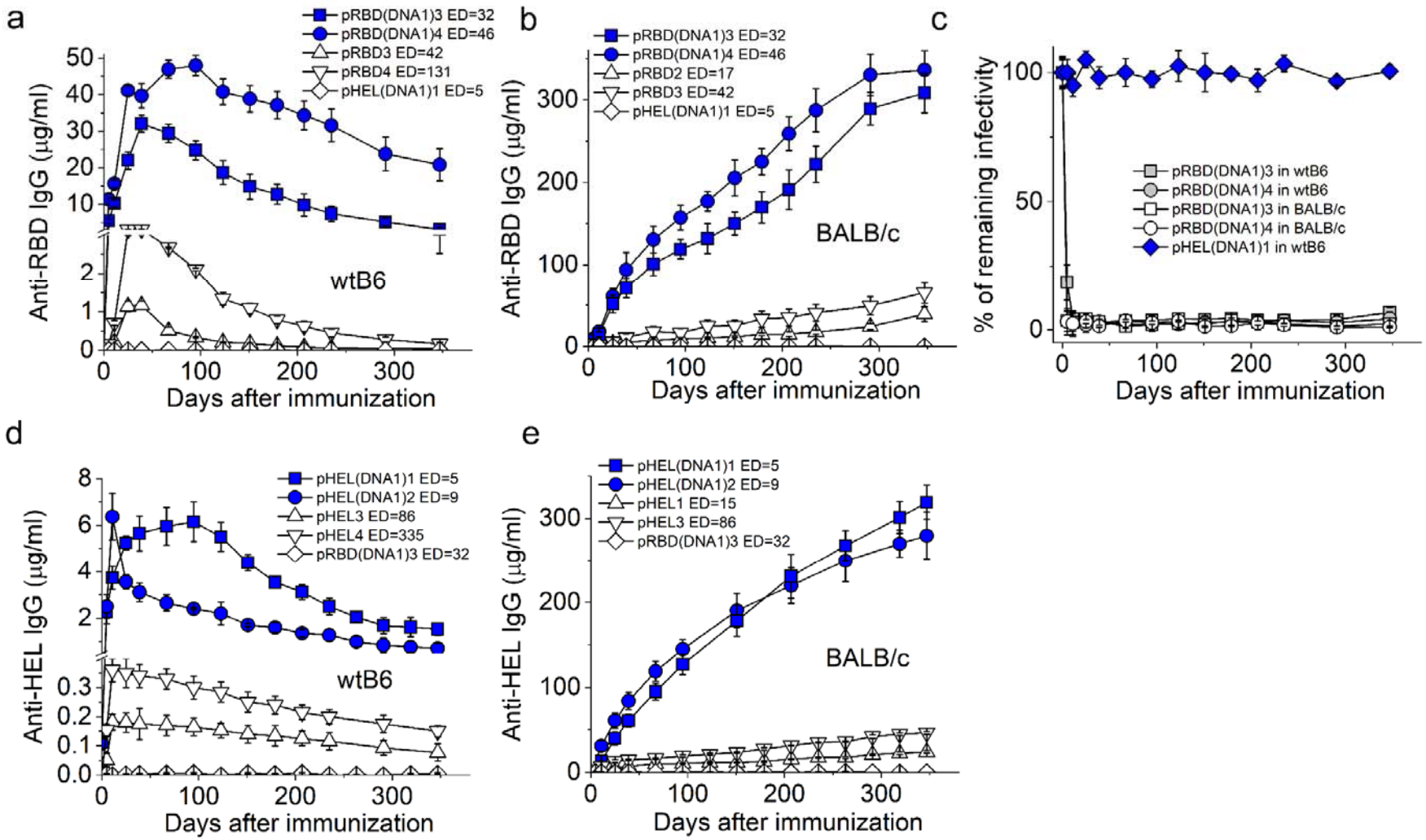
a
pRBD(DNA1)3 ED=32
pRBD(DNA1)4 ED=46
pRBD3 ED=42
pRBD4 ED=131
pHEL(DNA1)1 ED=5
Anti-RBD IgG (μg/ml)
wtB6
Days after immunization
b
pRBD(DNA1)3 ED=32
pRBD(DNA1)4 ED=46
pRBD2 ED=17
pRBD3 ED=42
pHEL(DNA1)1 ED=5
Anti-RBD IgG (μg/ml)
BALB/c
Days after immunization
c
% of remaining infectivity
pRBD(DNA1)3 in wtB6
pRBD(DNA1)4 in wtB6
pRBD(DNA1)3 in BALB/c
pRBD(DNA1)4 in BALB/c
pHEL(DNA1)1 in wtB6
Days after immunization
d
pHEL(DNA1)1 ED=5
pHEL(DNA1)2 ED=9
pHEL3 ED=86
pHEL4 ED=335
pRBD(DNA1)3 ED=32
Anti-HEL IgG (μg/ml)
wtB6
Days after immunization
e
pHEL(DNA1)1 ED=5
pHEL(DNA1)2 ED=9
pHEL1 ED=15
pHEL3 ED=86
pRBD(DNA1)3 ED=32
Anti-HEL IgG (μg/ml)
BALB/c
Days after immunization

Fig. 1. Duration of the IgG response induced by SVLS. (**a**)(**b**) and (**d**)(**e**) Concentrations of Ag-specific IgG in mouse sera collected on different days after a single injection of various agents listed in each inset, where (a) and (b) are for anti-RBD IgG in wtB6 (a) and BALB/c mice (b), respectively, and (d) and (e) are for anti-HEL IgG in wtB6 (d) and BALB/c mice (e), respectively. All concentrations were measured using ELISA based on standard curves obtained from mAb1 or mAb2. (**C**) Time courses of pseudovirion neutralization by various sera from immunized animals as listed in the inset. The doses of Ags for SVLS displaying RBD were 0.24 µg per animal. The dose of Ags for SVLS displaying HEL were 0.3 µg per animal for pHEL and 0.1 µg per animal for pHEL(DNA1), respectively. Throughout Fig. 1, N=4 for each time point.

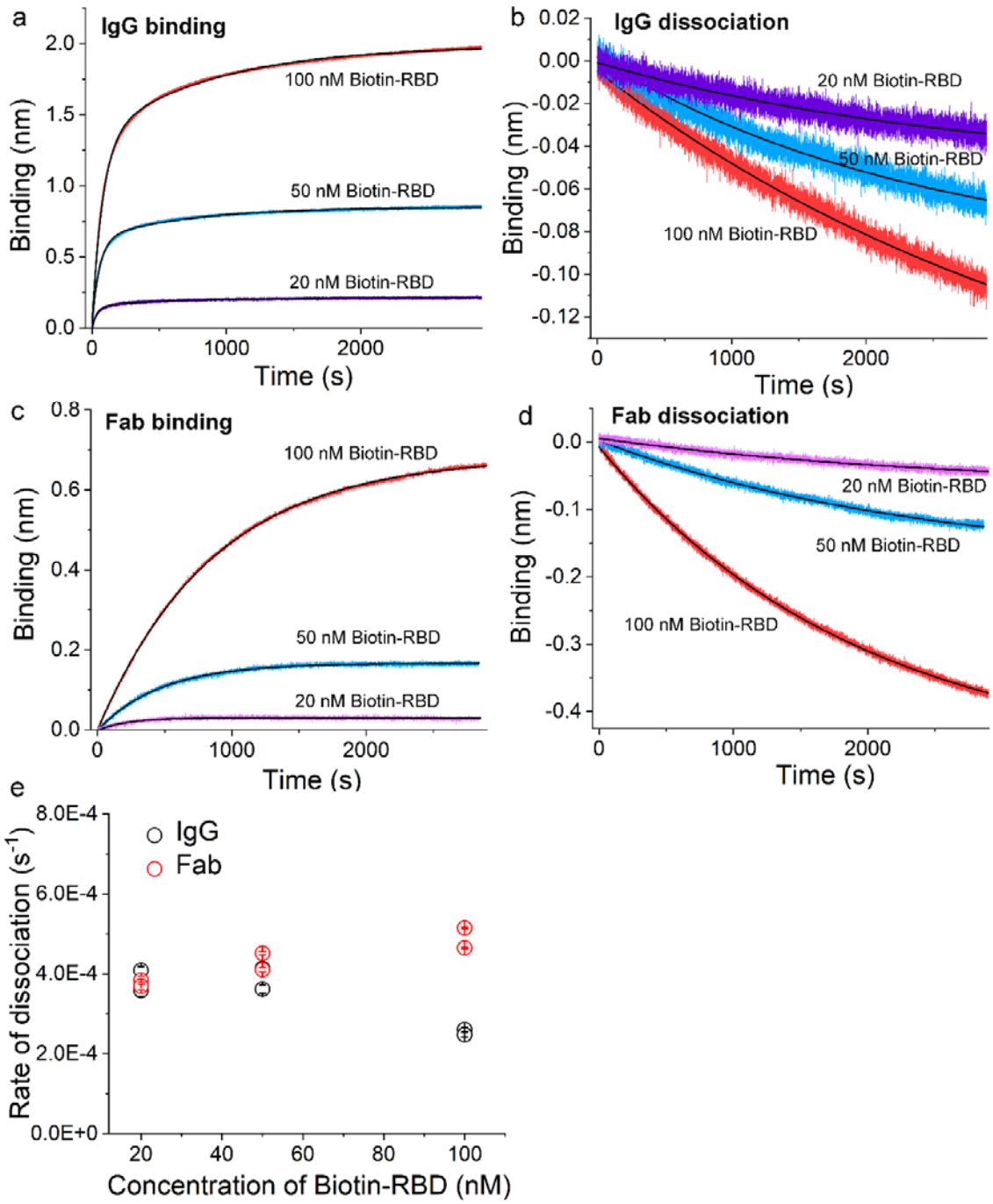

Fig 2. Validation of low-density coating of streptavidin sensors in BioLayer interferometry experiments. (**a**)(**b**) Real-time binding for mAb1 to biotin-RBD and its dissociation measured using BioLayer interferometry. The concentration of the IgG was 38 nM. (**c**)(**d**) Real-time binding for a Fab fragment to biotin-RBD and its dissociation measured using BioLayer interferometry. The concentration of the Fab was 62 nM. (a) through (d), the solid black lines were fits to both the binding and dissociation curves using exponential functions. (**e**) The observed rate constant of dissociation was plotted as a function of the concentration of biotin-RBD that was used to coat streptavidin sensors.

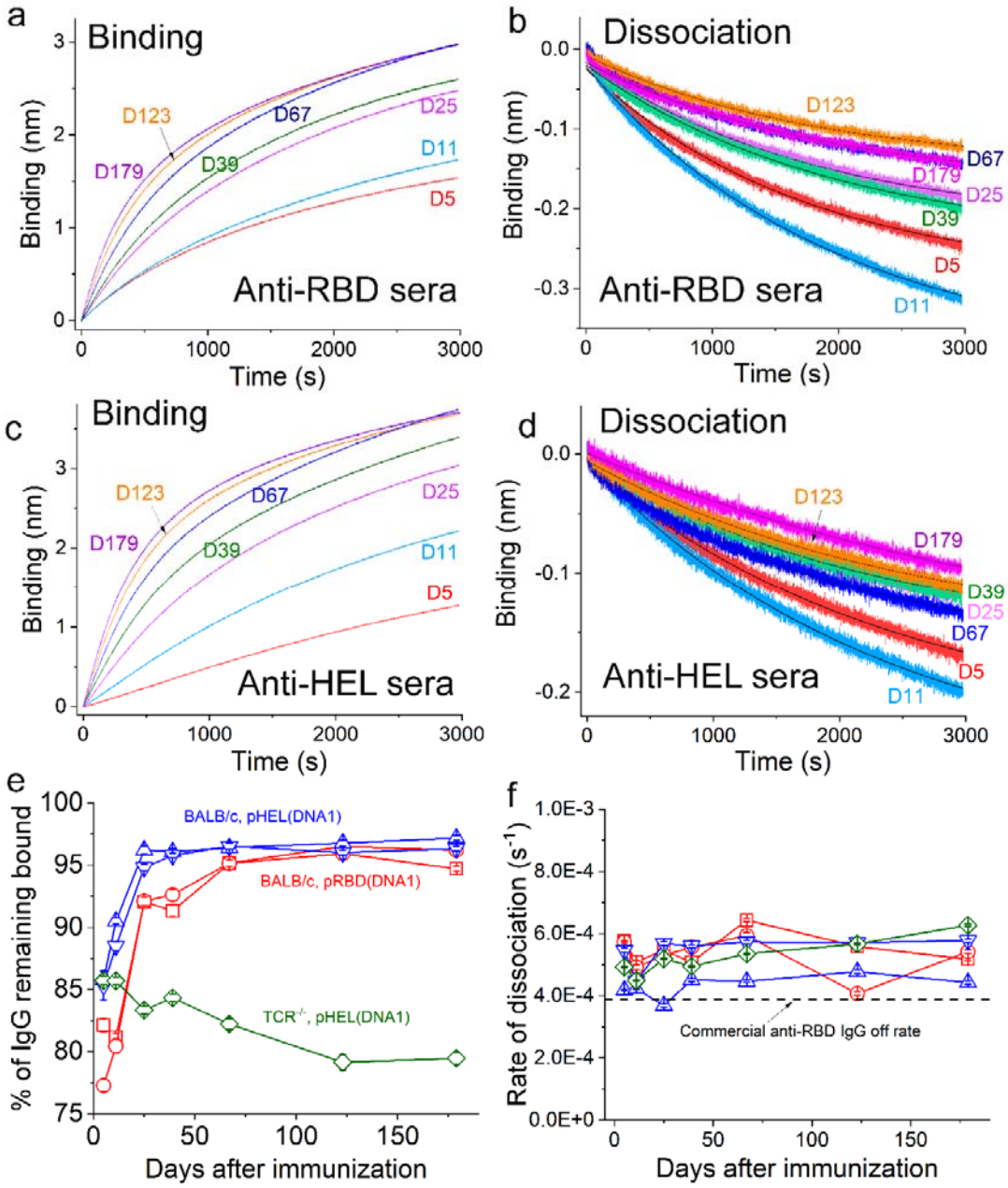

Fig. 3. Kinetics for the binding and dissociation of various Ag-specific sera samples monitored using BioLayer interferometry. (**a**)(**b**)(**c**) and (**d**) Real-time binding and dissociation measurements for mouse sera from different days after immunization using SVLS as described in the text. (**e**)(**f**), percent of IgG remaining bound at the end of dissociation (e) and the dissociation rates (f) as a function of days after immunization measured using BioLayer interferometry for sera samples from various immunization conditions as indicated in (e). For both (e) and (f), red squares, red circles, upper triangles, down triangles and diamonds represent sera samples from immunizations using pRBD(DNA1)3, pRBD(DNA1)4, pHEL(DNA1)1, pHEL(DNA1)2, and pHEL(DNA1)1 respectively. The doses of RBD and HEL were 0.24 and 0.1 µg per animal, respectively. N=4 for each time point in (e) and (f).

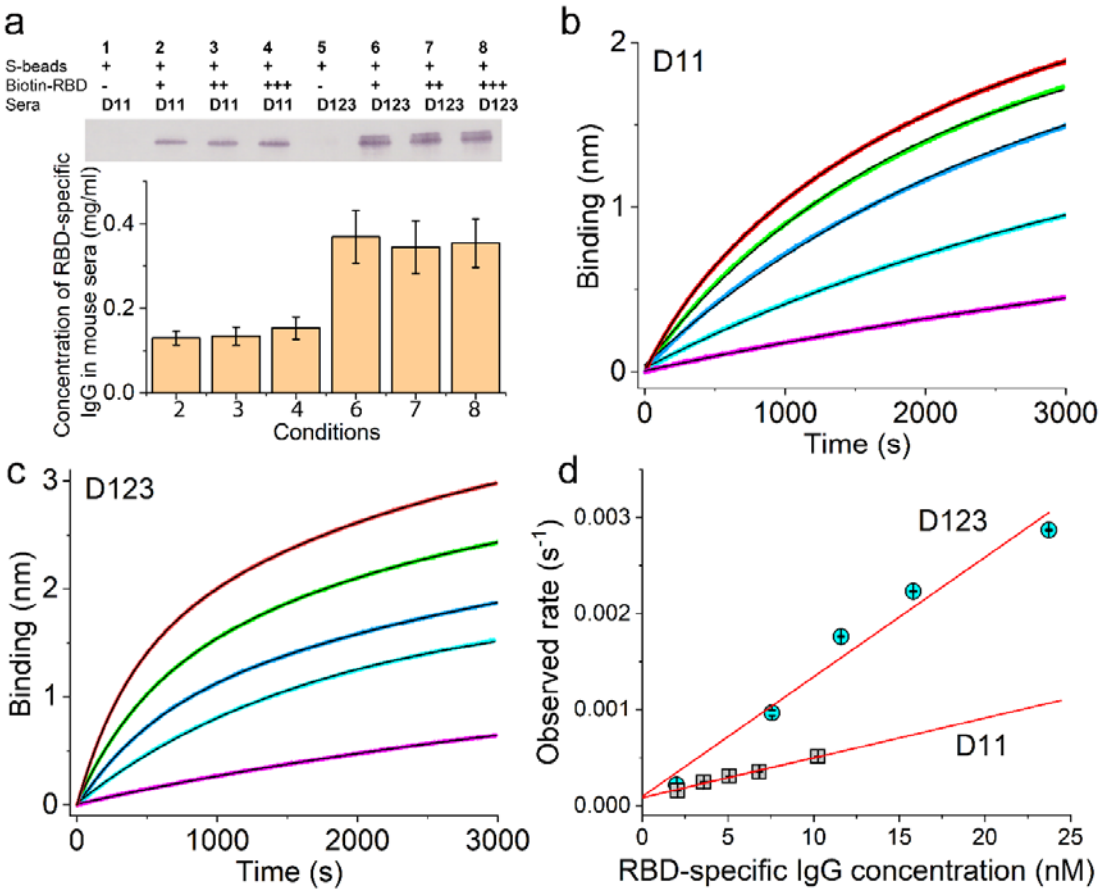

Fig. 4. Affinity maturation of the RBD-specific IgG response induced by pRBD(DNA1) in BALB/c mice. (**a**) RBD-specific IgG capture using streptavidin-coated magnetic beads together with biotin-RBD. (**b**)(**c**) Real-time binding curves between biotin-RBD and mouse sera at various dilutions, with (b) for sera collected on D11 and (c) for sera collected on D123 after the single injection. The dose of RBD was 0.24 µg per animal. The concentrations of RBD-specific IgG in each dilution are shown in panel (d) along the x-axis. The exponential fits are shown in black solid curves. (**d**) The observed binding rate constants with standard errors obtained from exponential fits of the binding curves shown in (b) and (c) are plotted as a function of RBD-specific IgG concentration for sera from D11 (grey squares) and sera from D123 (cyan circles). Adjusted R-square values from linear regressions are 0.987 for D11 and 0.960 for D123, respectively.

Additional Materials for

Minimal determinants for lifelong antiviral antibody responses from a single exposure to virus-like immunogens at low doses

Wei-Yun Wholey[1†], Alexander R. Meyer[1†], Sekou-Tidiane Yoda[1], Bryce Chackerian[2], Julie Zikherman[3], Wei Cheng[1,4]*

[1]*Department of Pharmaceutical Sciences, 428 Church Street, University of Michigan, Ann Arbor, Michigan 48109, USA*

[2]*Department of Molecular Genetics and Microbiology, School of Medicine, University of New Mexico, Albuquerque, New Mexico 87131, USA*

[3]*Division of Rheumatology, Rosalind Russell and Ephraim P. Engleman Rheumatology Research Center, Department of Medicine, University of California, San Francisco, California 94143 USA*

[4]*Department of Biological Chemistry, 1150 W. Medical Center Dr., University of Michigan Medical School, Ann Arbor, Michigan 48109, USA*

*Correspondence to: chengwe@umich.edu

The additional materials include:

Extended Data Figs. 1 to 3

Table S1

Extended Data Fig. 1. Lifelong IgG responses induced by SVLS(DNA1) in BALB/c mice.

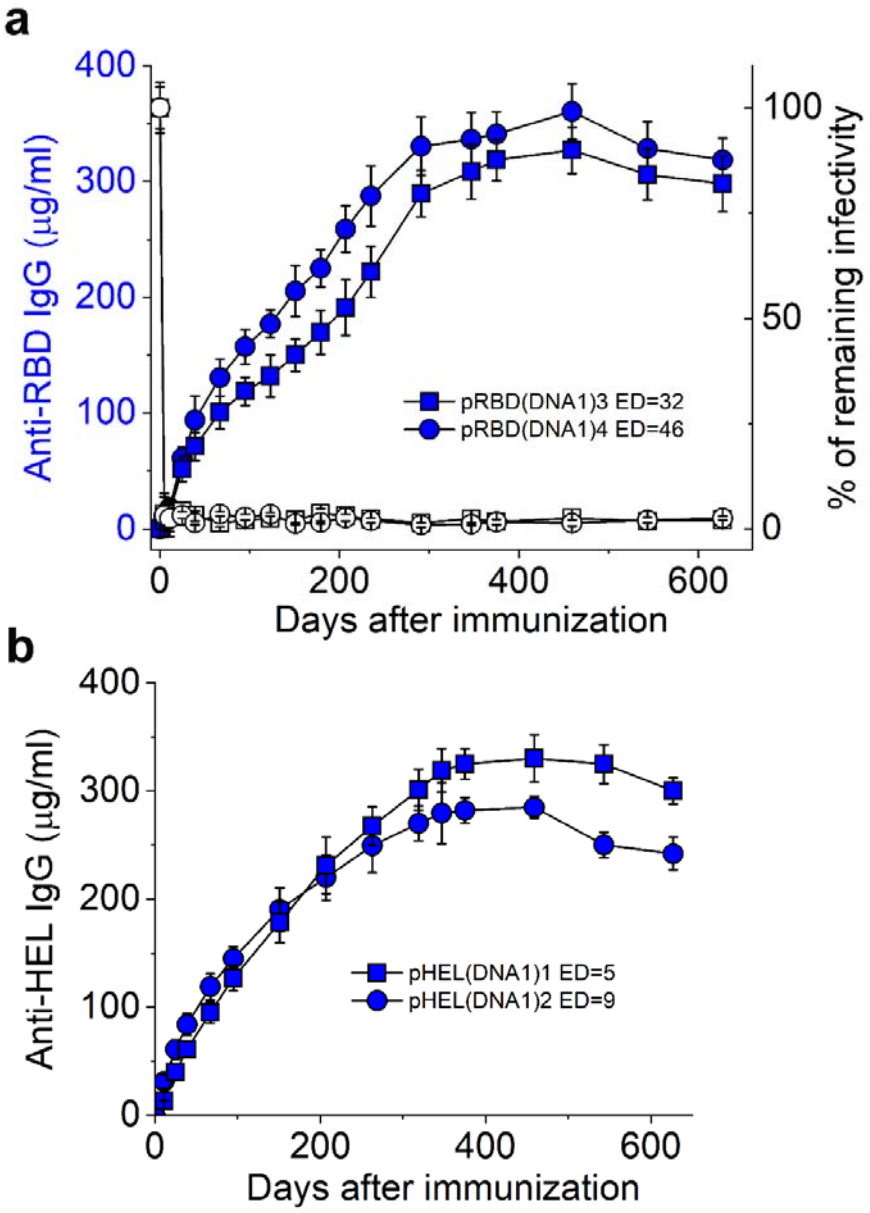

(a) Left y-axis and blue solid symbols: Concentrations for RBD-specific IgG as measured from ELISA for mouse sera collected on different days after a single injection of the respective agents in BALB/c mice as listed in the inset. **Right y-axis and white symbols**: time courses of pseudovirion neutralization by mouse sera from BALB/c mice after a single injection of the agents listed in the inset, with white squares for pRBD(DNA1)3 (ED=32) and white circles for pRBD(DNA1)4 (ED=46). The doses of RBD were 0.24 μg per animal. (**b**) Concentrations for HEL-specific IgG as measured from ELISA for mouse sera collected on different days after a single injection of the respective agents in BALB/c mice as listed in the inset, with blue squares for pHEL(DNA1)1 (ED=5) and blue circles for pHEL(DNA1)2 (ED=9). The doses of HEL were 0.1 μg per animal.

Extended Data Fig. 2. Indicator of affinity maturation that is largely independent of sera IgG concentrations.

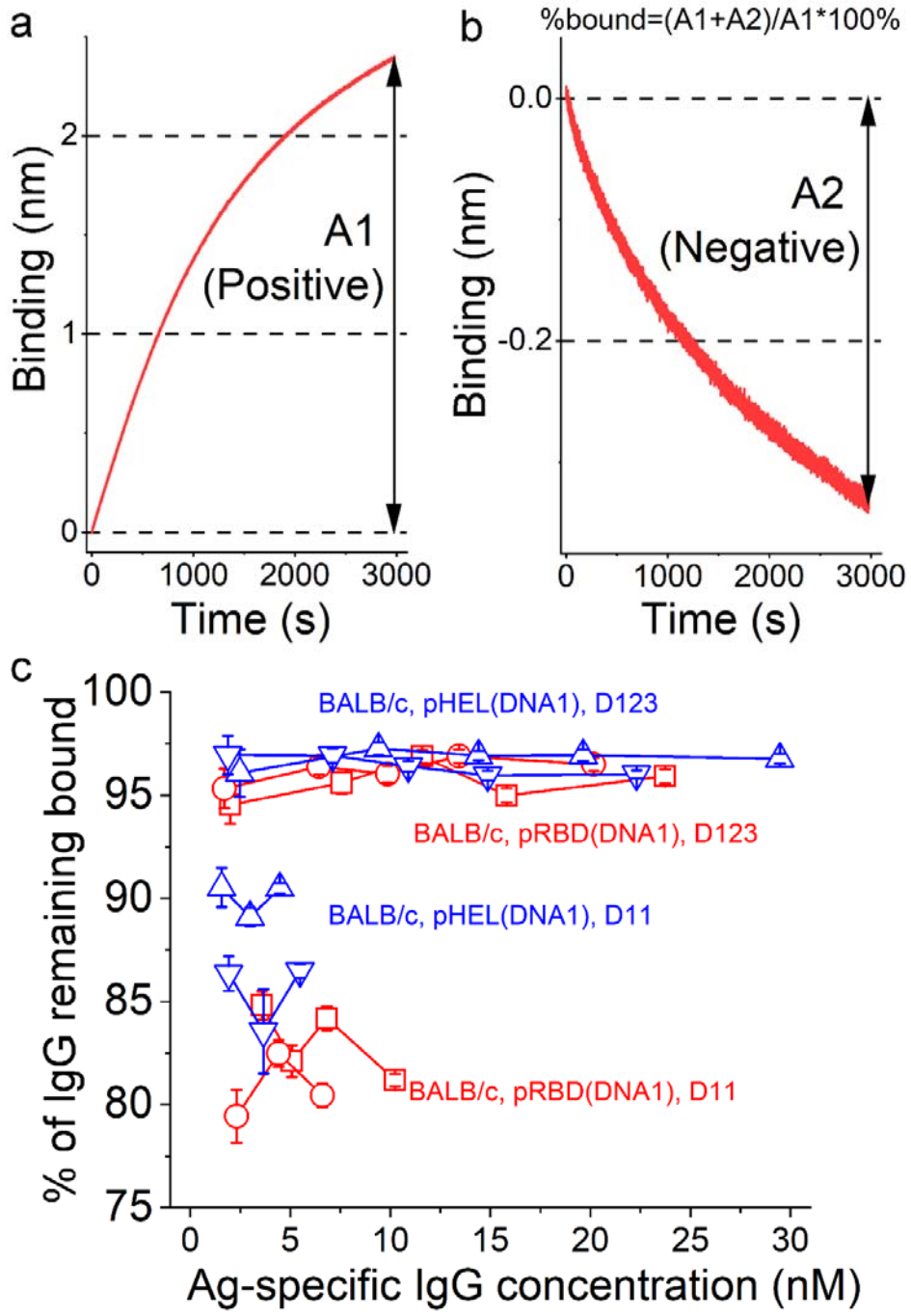

(**a**) A representative serum IgG binding curve showing the definition of binding amplitude, A1, that is measured from BioLayer interferometry experiments. A1 is the difference in the binding signal between the end and the beginning of a binding curve, which takes a positive value with a unit of nm. (**b**) The corresponding dissociation curve from (a) showing the definition of dissociation amplitude, A2, that is measured from BioLayer interferometry experiments. A2 is the difference in the binding signal between the end and the beginning of a dissociation curve, which takes a negative value with a unit of nm. The percentage of IgG

remaining bound at the end of dissociation is calculated as indicated on top of panel (b). (**c**) The percentage of IgG that remains bound at the end of dissociation was plotted as a function of the Ag-specific IgG concentration. For each color and symbol, the different concentrations were realized by dilution of the sera and then BioLayer interferometry experiments were conducted. This was done for several serum samples from BALB/c mice immunized with the agents as noted in the figure. Specifically, red squares, red circles, upper triangles, and down triangles are for pRBD(DNA1)3, pRBD(DNA1)4, pHEL(DNA1)1, and pHEL(DNA1)2, respectively. The dose of RBD was 0.24 µg per animal and the dose of HEL was 0.1 µg per animal. The concentrations for Ag-specific IgG were determined using magnetic beads capture as described in Materials and Methods. N=4 for each Ag-specific IgG concentration in (c).

Extended Data Fig. 3. A representative standard curve from quantitative western blots to determine the concentration of Ag-specific IgG in mouse sera.

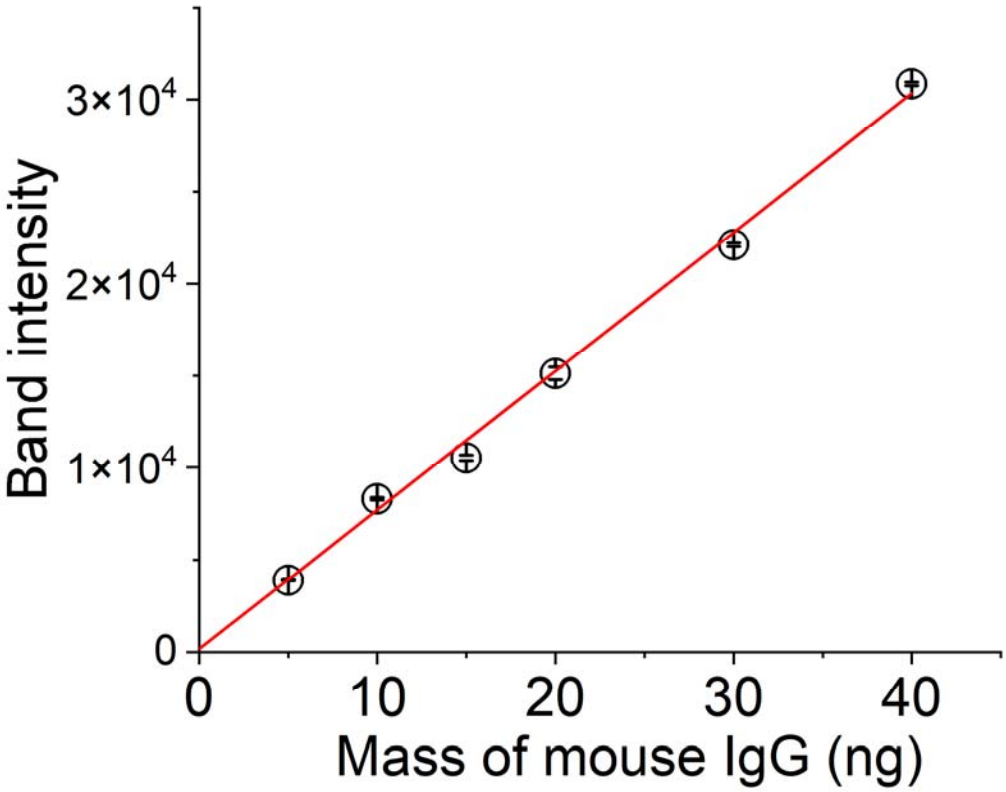

We used mAb1, a commercial monoclonal mouse IgG (BioLegend CAT#944803) as the known reference to construct a standard curve on the same western blot on which Ag-specific IgG antibodies captured by streptavidin magnetic beads were loaded. The band intensity was quantified using ImageJ and plotted against the loaded references (N=3 for each data point). A linear regression (the straight red line) was then used to quantitate the mass of Ag-specific IgG in serum samples. The adjusted R-square value from the linear regression as shown above is 0.998. The mass was then used to calculate the concentration of the IgG based on volume dilutions.

Table S1. A summary of key findings from the current study regarding the initiation and maintenance of a nAb response in mice upon a primary encounter with virus-like immunogens and their implications for understanding antiviral Ab responses.

Neutralizing antibody response →

SVLS type	Mouse strains	Initiation (by Day 5)	Amplification (by Day 11)	Duration (Day 12 to 300+)
High ED, no iNA 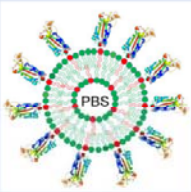	B6	Yes	Yes, but limited compared to BALB/c	Wane with time
		IgG1 IgG2b IgG3 T-cell independent CD19 dependent, MyD88 independent		
	BALB/c	Yes	Yes, with strong IgG1	Grow with time
		IgG1 IgG2b IgG3		
Low ED, with iNA 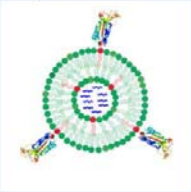	B6	Yes	Yes	Wane with time, but a stronger response than SVLS without iNA
		IgG1 IgG2b IgG2c IgG3 T-cell independent Can be CD19 independent, TLR/MyD88 dependent		
	BALB/c	Yes	Yes	Grow with time, and a stronger response than SVLS without iNA
		IgG1 IgG2a IgG2b IgG3		

Based on current studies, we divide the time dependence of a nAb response into three segments: initiation (by D5), amplification (by D11) and duration (D12 to 300 and beyond). Both SVLS with high ED but without iNA and SVLS with low ED and iNA can induce nAb responses in either B6 or BALB/c mice, although the details in terms of initiation, amplification and duration are different. For SVLS of high ED but without iNA, they initiate a nAb response in B6 mice and the animals produce IgG1, IgG2b and IgG3, like that in BALB/c mice, but the amplification of the nAb response is limited compared to that in BALB/c mice. The nAb level also wanes with time, which contrasts with the nAb response in BALB/c mice that grows with time. BALB/c mice have more IgG1 produced during the stage of amplification. These nAb responses in B6 mice are largely T-cell independent and MyD88 independent but depend on CD19 as revealed by experiments in gene knockout mice of B6 background. For SVLS of low ED with iNA, they initiate nAb responses in both B6 and BALB/c mice and the animals produce IgG1, IgG2c/2a, IgG2b and IgG3. Both initiation and amplification are similar in these two strains of mice, although the quantitative trends in the long-term are different. The nAb response wanes with time in B6 mice but grows with time in BALB/c mice. For both strains, the nAb responses are much stronger than the responses induced by SVLS without iNA. These nAb responses in B6 mice depend on TLRs and MyD88 but are largely T-cell independent and can be even mounted in the absence of CD19 as revealed by experiments in gene knockout mice of B6 background. Ag-specific B cells integrate both features of viral signals, i.e., ED and iNA, from individual virus-like

immunogens to initiate a nAb response. The intrinsic sensing of iNA by TLRs can profoundly modulate the magnitudes of the Ab response in both the short and long term.

These data explain key features of the nAb response in live viral infections, including its speed[48], its duration, the types of nAb class switching observed, and the T cell independence of the immediate but potent nAb response[49-52] that does not require somatic hypermutation or affinity maturation[30].

Lastly, it is important to note that the potency of secreted IgG to neutralize viruses can be affected by ED from the perspective of IgG binding avidity. While low ED on the surface of SVLS with iNA can activate antigen-specific B cells and lead to strong IgG secretion, low ED on the surface of virions can also adversely affect the neutralization potency of the secreted IgG[34]. This is because a low ED on virion surfaces can impede the bivalent binding of IgG, thereby reducing binding avidity, as has been demonstrated for HIV-1[35].